51st AIAA Aerospace Sciences Meeting including the New Horizons Forum and Aerospace Exposition
07 - 10 January 2013, Grapevine (Dallas/Ft. Worth Region), Texas

AIAA 2013-0984

LES Study of Shock Wave and Turbulent Boundary Layer Interaction

Justine Li,* Nathan Grube,† Stephan Priebe,‡
and M. Pino Martín§

The large eddy simulation (LES) of a compression ramp shock wave and turbulent boundary layer interaction (STBLI) is presented. The ramp angle is 24° and the incoming boundary layer flow conditions are Mach 2.9 and Re_θ 2900. The LES data are in good agreement with existing direct numerical simulation (DNS) data with the same incoming flow parameters. The accuracy and reduced resolution requirements of the LES as compared to the DNS enables the ability to resolve the aperiodic cycle of the low-frequency unsteadiness characteristic of these flows.

Nomenclature

p	pressure
ρ	density
T	temperature
u, v, w	streamwise, spanwise, and wall-normal velocity
U_∞	freestream velocity
u_τ	friction velocity
μ	dynamic viscosity
ν	kinematic viscosity
M	Mach number
δ	99% boundary layer thickness
δ^*	compressible displacement thickness
θ	compressible momentum thickness
Re_θ	Reynolds number based on momentum thickness, θ, and freestream values U_∞ and ν_∞
C_f	skin-friction coefficient
i, j, k	computational coordinates in streamwise, spanwise, and wall-normal directions
x, y, z	physical coordinates in streamwise, spanwise, and wall-normal directions
C_k^r	optimal weight for stencil k, using r grid points
ω_k	weight of stencil k
IS_k	smoothness measurement index of stencil k
TV_k	total variation of flux over stencil k

Superscript

$*$	coordinates referenced to compression corner location
$+$	nondimensionalization by inner units, ν_w/u_τ

Subscript

w	wall quantity
∞	freestream quantity

*Graduate Student, Department of Aerospace Engineering, University of Maryland, College Park.
†Faculty Research Assistant, Department of Aerospace Engineering, University of Maryland, College Park.
‡Research Assistant, Department of Aerospace Engineering, University of Maryland, College Park.
§AIAA Associate Fellow. Associate Professor, Department of Aerospace Engineering, University of Maryland, College Park.

I. Introduction

The interaction of a shock wave with a turbulent boundary layer is a common and important flow feature in many compressible flow applications. A key physical aspect of STBLIs is the low-frequency unsteadiness that occurs when the mean-flow is separated. If U_∞/δ is the characteristic frequency of the energetic scales in the inflow boundary layer, then the characteristic frequency of the shock motion will typically be 1 to 2 orders of magnitude lower, i.e. $O(0.1 - 0.01U_\infty/\delta)$.[1,2]

The cause of the low-frequency unsteadiness is still under debate. It has been proposed that the shock motion is due to the upstream boundary layer, see e.g. Ganapathisubramani, Clemens and Dolling,[3] or, alternatively, that it is due to the downstream separated flow, see e.g. Dupont et al.,[4] Dussauge et al.,[5] and Piponniau et al.[6]

Recent large eddy simulations (LESs) and direct numerical simulations (DNSs) capture the low-frequency unsteadiness. The ability of LES to capture the important physical aspects of STBLI flows has been demonstrated (e.g. Garnier, Sagaut and Deville,[7] Loginov, Adams and Zheltovodov,[8] and Morgan, Kawai and Lele[9]). Touber and Sandham[10] performed the LES of a reflected STBLI at Mach 2.3 and Re_θ 5900, matching experimental flow conditions.[5] The low-frequency unsteadiness is present in their simulations at the same frequency as in experiments. They use a new inflow technique to ensure that no artificial low-frequency forcing is introduced into the computation. A stability analysis is also performed, and this shows the presence of a global instability mode which could be connected to the observed low-frequency unsteadiness. Wu and Martín[11,12] performed the DNS of a 24° compression ramp at Mach 2.9 and Re_θ 2300. They validated their results (in terms of separation length, mean wall-pressure distribution, evolution of the mean flow through the interaction) against experiments by Bookey et al.[13,14] at matching conditions. In addition, Ringuette, Wu and Martín[15] validated the fluctuating wall-pressure in the DNS against the experiments by Ringuette and Smits.[16,17] The shock motion was inferred in the DNS from wall-pressure fluctuations, and mass-flux fluctuations in the freestream, and its frequency was found to agree with a scaling previously proposed.[5] Priebe and Martín[18] describe the low-frequency dynamics from the temporal evolution of low-pass filtered DNS flow fields and find evidence that structural changes occur in the downstream separated flow during the low-frequency motion. They show that the observed structural changes are reminiscent of the global linear instability mode described by Touber and Sandham.

The LES data of the Mach 2.9 Re_θ 2900 flow for the 24° compression ramp configuration and validation against existing DNS data for the same conditions are presented. In Section II, the numerical methods used in the LES are presented. Section III describes the computational domain, boundary conditions and initial conditions. The results of the incoming turbulent boundary layer and the time- and spanwise-averaged compression ramp flow are presented in Section IVA and IVB respectively. Evidence of the shock motion and wall-pressure fluctuations characteristic of STBLI flows is shown in Section IVC. Validation of the LES data demonstrates progress towards its capability to capture flow features seen in the DNS data at a significantly reduced computational cost.

II. Numerical Methods

The LES solves the Favre-filtered Navier-Stokes equations (1) - (3) where the Favre-filter is defined as $\widetilde{f} = \overline{\rho f}/\overline{\rho}$. The resolved, large-scale variable is defined as $\overline{f}(x) = \int_D f(x')G(x, x' : \overline{\Delta})dx'$, where D is the domain, G is the filter function, and $\overline{\Delta}$ is the filter-width. The diffusive fluxes are defined as $\breve{\sigma}_{ij} = 2\mu S_{ij} - \frac{2}{3}\mu\delta_{ij}S_{kk}$, E is the total energy, γ is the ideal heat capacity ratio for dry air, and c_v is the heat capacity at constant volume. On the right hand side of the Favre-filtered Navier-Stokes equations, the subgrid scale stresses $\tau_{ij} = \overline{\rho}(\widetilde{u_i u_j} - \widetilde{u}_i\widetilde{u}_j)$, and heat flux $Q_j = \overline{\rho}(\widetilde{u_j T} - \widetilde{u}_j\widetilde{T})$ are modeled using the one-coefficient dynamic mixed model. The subgrid scale turbulent kinetic energy diffusion term $J_j = \overline{\rho}(u_j\widetilde{u_k u_k} - \widetilde{u}_j\widetilde{u_k u_k})$ is modeled using the model by Knight et al., 1998.[19] The subgrid scale viscous diffusion term, D_j, is not modeled due to its small contribution compared to the other subgrid scale terms. Further information on the subgrid scale models used here is provided in Martín, Piomelli and Candler.[20]

$$\frac{\partial\overline{\rho}}{\partial t} + \frac{\partial}{\partial x_j}(\overline{\rho}\widetilde{u_j}) = 0 \tag{1}$$

$$\frac{\partial}{\partial t}(\overline{\rho}\widetilde{u_i}) + \frac{\partial}{\partial x_j}(\overline{\rho}\widetilde{u_i}\widetilde{u_j} + \overline{p}\delta_{ij} - \breve{\sigma}_{ij}) = -\frac{\partial}{\partial x_j}\tau_{ij} \tag{2}$$

$$\frac{\partial}{\partial t}(\overline{E}) + \frac{\partial}{\partial x_j}\left[(\overline{E}+\overline{p})\widetilde{u_j} + \breve{q_j} - \breve{\sigma}_{ij}\tilde{u}_i\right] = -\frac{\partial}{\partial x_j}(\gamma c_v Q_j + \frac{1}{2}J_j - D_j) \tag{3}$$

The governing equations are solved using a curvilinear finite difference code. The viscous fluxes and the subgrid scale terms are discretized using 4th order central difference scheme. Time integration is performed using 3rd-order, low-storage Runge-Kutta method.[21]

The inviscid fluxes are discretized using a shock-capturing Weighted Essentially Non-Oscillatory (WENO) method, linearly and nonlinearly optimized. The flux terms are computed using a modified fourth-order bandwidth-optimized WENO method with limiters. The limiters are used in the smoothness measurement which determines the existence of a discontinuity within the stencil over which the flux is computed. In order to prevent excessive numerical dissipation in the flowfield, absolute and relative limiters, (4) and (5) respectively, are used together in determining the weight of each stencil. The impact of using these limiters is shown through 2D nonlinearity index contour plots, where the nonlinearity index (NI) is defined as (6). The NI ranges from 0 to 1 such that it is nonzero for regions near discontinuities in flowfield values. For both the simulation and Figure 2, the threshold values are $A_{AL} = 0.0001$, $A_{RL}^{TV} = 4.5$, and $B_{RL}^{TV} = 0.2$. These limiter thresholds are different from those used in a previous DNS.[11] In Figure 1, the nonlinearity index without the use of limiters is calculated for an instantaneous flowfield showing excessive dissipation in the entire boundary layer throughout the flowfield, decreasing the accuracy of the simulation. Figure 2 shows the nonlinearity index after both the absolute and relative limiters have been applied, showing numerical dissipation at the shock while decreasing dissipation within the boundary layer. In this case, the nonlinearity index remains high within and downstream of the separated region, which leads to errors in the wall-pressure distribution as described in Section IVB. A more in-depth explanation of the WENO method used here is provided in Martín, Taylor, Wu and Weirs,[22] Taylor, Wu and Martín 2007,[23] Wu and Martín, 2007,[11] and Grube and Martín.[24]

$$\omega_k = \begin{cases} C_k^r, & \text{if } max(IS_k) \le A_{AL} \\ \omega_k, & \text{otherwise} \end{cases} \tag{4}$$

$$\omega_k = \begin{cases} C_k^r, & \text{if } max(TV_k)/min(TV_k) \le A_{RL}^{TV} \text{ and } max(TV_k) \le B_{RL}^{TV} \\ \omega_k, & \text{otherwise} \end{cases} \tag{5}$$

$$NI = \frac{1}{(r(r+1))^{1/2}}\left[\sum_{k=0}^{r}\left(\frac{[1/(r+1)] - [(\omega_k/C_k^r)/\sum_{k=0}^{r}(\omega_k/C_k^r)]}{[1/(r+1)]}\right)^2\right]^{1/2} \tag{6}$$

III. Computational Setup

The LES is performed on a grid consisting of $288 \times 40 \times 64$ points in the streamwise, spanwise, and wall-normal directions for a total of approximately 0.74 million points, a 96% reduction in the number of points as compared to the DNS of the same flow. The grid is generated using the analytical method described in Wu and Martín[25] such that the grid points are clustered at the wall and at the corner. The grid resolution in the streamwise direction is $\Delta x_{max}^+ = 32.4$ and $\Delta x_{min}^+ = 13.5$. The grid spacing is uniform in the spanwise direction such that $\Delta y^+ = 16.7$. The first point above the wall is $\Delta z_1^+ = 0.38$. The dimensions of the computational domain are shown in Figure 3. This domain has approximately the same dimensions as the DNS presented in Wu and Martín, 2007.[11]

At the inlet, the rescaling method for compressible flows described in Xu and Martín[26] is used to generate continuous inflow data from a streamwise location upstream from the interaction region and far enough downstream such that the autocorrelation of the streamwise velocity decays to zero. This rescaling length of 5.07δ is sufficiently long to satisfy the Eulerian decorrelation criterion described in Priebe and Martín.[18] Due to the spurious correlation in the short rescaling box, the freestream flow has been filtered at the inlet to eliminate acoustic noise outside of the boundary layer. The outlet has a supersonic exit boundary condition, and the top boundary has a freestream boundary condition. Periodic boundary conditions are applied in the spanwise direction. The wall boundary condition is isothermal where $T_w = 307K$. The dynamic viscosity, μ, is defined using Sutherland's formula in the entire flowfield.

The compression ramp flow is initialized using DNS data from a turbulent boundary layer simulation

with the same incoming flow parameters. The DNS data is filtered to LES resolution using a tophat filter described in Martín, Piomelli and Candler.[27] In this case, the LES turbulent boundary layer data has a factor of 4 fewer points in the streamwise and spanwise directions and a factor of 2 fewer points in the wall-normal direction. In Figure 4, it can be seen that approximately 15% of the turbulent kinetic energy is contained in the subgrid scales. The filtered TBL data is then interpolated onto the compression ramp curvilinear grid.

IV. Results

A. Incoming Boundary Layer

The Mach number, M, is defined as the freestream velocity, U_∞, divided by the freestream speed of sound. The momentum thickness, θ and the displacement thickness, δ^*, are computed using compressible definitions. The Reynolds number, $Re_\theta = U_\infty \theta / \nu_\infty$, is based on the momentum thickness and freestream quantities for velocity and dynamic viscosity, and H is the shape factor. The values of the incoming boundary layer flow parameters are shown below in Table 1.

Table 1. Flow parameters of incoming fully turbulent boundary layer

	M	Re_θ	θ [mm]	δ^* [mm]	H	C_f
LES	2.92	2.9×10^3	0.54	2.42	4.48	0.00187
DNS[18]	2.91	2.9×10^3	0.47	2.58	5.49	0.00219

B. Time- and Spanwise-averaged Results

Statistics of the flow are gathered over $350\delta/U_\infty$ at a frequency of approximately $1U_\infty/\delta$. This is approximately the same simulation length used in validating the DNS of the STBLI compression ramp configuration presented in Wu and Martín, 2007.[11] In Figure 5, an instantaneous numerical schlieren plot from the LES data shows the same flow features seen in the DNS data; the turbulence structures in the incoming boundary layer are of a similar length, the turbulence is amplified downstream of the main shock, and the main shock exhibits wrinkling.

The separation length is determined from the time- and spanwise-averaged distribution of C_f in Figure 6a. The superscript '*' denotes the streamwise coordinate measured along the wall with the origin at the corner of the compression ramp such that $x^*/\delta = 0$. The separation point is $x^*/\delta = -2.1$ which is identical to the DNS result, and the reattachment point is $x^*/\delta = 0.66$, slightly upstream of the DNS result and leading to a decrease in separation length of about 7%. Within the separated flow region, inflection points near the separation point and within the separated region in the C_f distribution indicates that the LES captures the same flow features seen in the DNS of the same configuration. The wall-pressure distribution, shown in Figure 6b, shows agreement at the inlet as well as at recovery well downstream of the compression corner. In the separated flow region, the pressure plateau characteristic for STBLI does not fully develop, causing an overprediction of the wall-pressure immediately downstream of the separation point. The undeveloped wall-pressure plateau in the DNS data was attributed to the need for different threshold values for the absolute and relative limiters used in the implemented WENO method described in Section II.[28] Taylor, Wu and Martín[23] completed an in-depth study to determine limiter values that were robust for the given numerical methods on DNS grids. A similar study has not been carried out for LES resolution grids.

The maximum mass-flux turbulence intensity, in Figure 7, shows an amplification of a factor of 4.5 downstream of the interaction as compared to the upstream value. This is consistent with the results for the similar flow configuration presented in Wu and Martín, 2007[11] in which the mass-flux turbulence intensity amplification is found to be predominately a result of the pressure rise, which in turn is determined by the compression ramp angle and the Mach number.

C. Shock motion and wall-pressure fluctuation

Shock motion is inferred from the wall-pressure signal. In Figure 8, the wall-pressure signal is shown for the incoming boundary layer -5.9δ upstream of the compression corner, for the time- and spanwise-averaged separation point at -2.1δ, and inside the separated region at -1.1δ. For both the wall-pressure signals at the mean separation point and inside the separated region, the values exhibit a high-frequency fluctuation and a low-frequency fluctuation on the order of $O(0.01U_\infty/\delta)$, corresponding to a shock Strouhal number of 0.028. While this data only captures a couple of these periods, it is evident that this implementation of LES is capable of resolving the aperiodic low-frequency cycle in a dataset that spans a longer time period.

V. Conclusion

The LES data for the Mach 2.9 Re_θ 2900 shows good agreement to existing DNS data for the same incoming flow conditions. Using 96% fewer points than the DNS,[18] the LES data is able to capture characteristic flow features of a compression ramp flow. An instantaneous numerical schlieren qualtitatively shows the turbulent structures in the flowfield as well as the shock. The time- and spanwise-averaged friction coefficient shows similar structure within the separation bubble and accurately predicts the separation and reattachment points. The mass-flux turbulence intensity shows the same increase across the shock as seen in DNS data with the same flowfield configuration.[11] This short dataset demonstrates progress towards the LES capability of capturing the low-frequency unsteadiness characteristic of STBLI flows.

Acknowledgments

This work is supported by the Air Force Office of Scientific Research under grant AF/9550-10-1-0164 and by the Department of Defense through the National Defense Science and Engineering Graduate Fellowship Program.

References

[1]Smits, A. J. and Dussauge, J. P., *Turbulent Shear Layers in Supersonic Flow*, Springer Verlag, New York, 2nd ed., 2006.

[2]Dolling, D., "Fifty Years of Shock-Wave/Boundary-Layer Interaction Research: What Next?" *AIAA Journal*, Vol. 39, No. 8, 2001, pp. 1517–1531.

[3]Ganapathisubramani, B., Clemens, N. T., and Dolling, D. S., "Effects of upstream boundary layer on the unsteadiness of shock-induced separation," *Journal of Fluid Mechanics*, Vol. 585, 2007, pp. 369–394.

[4]Dupont, P., Haddad, C., and Debiève, J. F., "Space and time organization in a shock-induced separated boundary layer," *Journal of Fluid Mechanics*, Vol. 559, 2006, pp. 255–277.

[5]Dussauge, J. P., Dupont, P., and Debiève, J. F., "Unsteadiness in Shock Wave Boundary Layer Interactions with Separation," *Aerospace Science and Technology*, Vol. 10, No. 2, 2006.

[6]Piponniau, S., Dussauge, J., Debiève, J., and Dupont, P., "A simple model for low-frequency unsteadiness in shock-induced separation," *Journal of Fluid Mechanics*, Vol. 629, 2009, pp. 87–108.

[7]Garnier, E., Sagaut, P., and Deville, M., "Large Eddy Simulation of Shock/Boundary-Layer Interaction," *AIAA Journal*, Vol. 40, No. 10, 2002, pp. 1935–1944.

[8]Loginov, M. S., Adams, N. A., and Zheltovodov, A. A., "Large-eddy simulation of shock-wave/turbulent-boundary-layer interaction," *Journal of Fluid Mechanics*, Vol. 565, 2006, pp. 135–169.

[9]Morgan, B., Kawai, S., and Lele, S. K., "Large-Eddy Simulation of an Oblique Shock Impinging on a Turbulent Boundary Layer," *AIAA Paper No. 2010-4467*, June 2010.

[10]Touber, E. and Sandham, N., "Large-eddy simulation of low-frequency unsteadiness in a turbulent shock-induced separation bubble," *Theoretical and Computational Fluid Dynamics*, Vol. 23, 2009, pp. 79–107.

[11]Wu, M. and Martín, M. P., "Direct Numerical Simulation of Supersonic Turbulent Boundary Layer over a Compression Ramp," *AIAA Journal*, Vol. 45, No. 4, 2007, pp. 879–889.

[12]Wu, M. and Martín, M. P., "Analysis of Shock Motion in Shockwave and Turbulent Boundary Layer Interaction using Direct Numerical Simulation Data," *Journal of Fluid Mechanics*, Vol. 594, 2008, pp. 71–83.

[13]Bookey, P. B., Wyckham, C., Smits, A. J., and Martín, M. P., "New Experimental Data of STBLI at DNS/LES Accessible Reynolds Numbers," *AIAA Paper No. 2005-309*, Jan. 2005.

[14]Bookey, P. B., Wyckham, C., and Smits, A. J., "Experimental Investigations of Mach 3 Shock-Wave Turbulent Boundary Layer Interactions," *AIAA Paper No. 2005-4899*, June 2005.

[15]Ringuette, M. J., Wu, M., and Martín, M. P., "Low Reynolds Number Effects in a Mach 3 Shock Turbulent Boundary Layer Interaction," *AIAA Journal*, Vol. 46, No. 7, 2008.

[16]Ringuette, M. J. and Smits, A. J., "Wall-Pressure Measurements in a Mach 3 Shock-Wave and Turbulent Boundary Layer Interaction at a DNS-Accessible Reynolds Number," *AIAA Paper No. 2007-4113*, June 2007.

[17]Ringuette, M. J., Bookey, P., Wyckham, C., and Smits, A. J., "Experimental Study of a Mach 3 Compression Ramp Interaction at $Re_\theta = 2400$," *AIAA Journal*, Vol. 47, 2009, pp. 373–385.

[18]Priebe, S. and Martín, M. P., "Low-frequency unsteadiness in shock wave-turbulent boundary layer interaction," *Journal of Fluid Mechanics*, Vol. 699, 2012.

[19]Knight, D., Zhou, G., Okong'o, N., and Shukla, V., "Compressible Large Eddy Simulation Using Unstructured Grids," *AIAA Paper No. 98-0535*, 1998.

[20]Martín, M. P., Piomelli, U., and Candler, G. V., "Subgrid-scale Models for Compressible LES," *Theoretical and Computational Fluid Dynamics*, Vol. 13, 2000.

[21]Williamson, J. H., "Low-storage Runge-Kutta Schemes," *Journal of Computational Physics*, Vol. 35, No. 1, 1980, pp. 48–56.

[22]Martín, M. P., Taylor, E. M., Wu, M., and Weirs, V. G., "A Bandwidth-Optimized WENO Scheme for the Direct Numerical Simulation of Compressible Turbulence," *Journal of Computational Physics*, Vol. 220, 2006, pp. 270–289.

[23]Taylor, E. M., Wu, M., and Martín, M. P., "Optimization of Nonlinear Error Sources for Weighted Essentially Non-oscillatory Methods in Direct Numerical Simulations of Compressible Turbulence," *Journal of Computational Physics*, Vol. 223, 2007, pp. 384–397.

[24]Grube, N. and Martín, M. P., "Assessment of Subgrid-Scale Models and Shock-Confining Filters in Large-Eddy Simulation of Highly Compressible Isotropic Turbulence," *AIAA Paper No. 2009-0947*, 2009.

[25]Wu, M. and Martín, M. P., "Direct Numerical Simulation of Shockwave/Turbulent Boundary Layer Interaction," *AIAA Paper No. 2004-2145*, 2004.

[26]Xu, S. and Martín, M. P., "Inflow Boundary Conditions for Compressible Turbulent Boundary Layers," *AIAA Paper No. 2003-3963*, 2003.

[27]Martín, M. P., Piomelli, U., and Candler, G. V., "A Priori Test of SGS Models in Compressible Turbulence," *ASME Symposium on Transitional and Turbulent Compressible Flow*, ASME, San Francisco, CA, 1999.

[28]Wu, M. and Martín, M. P., "Assessment of Numerical Methods for DNS of Shockwave/Turbulent Boundary Layer Interaction," *AIAA Paper No. 2006-717*, 2006.

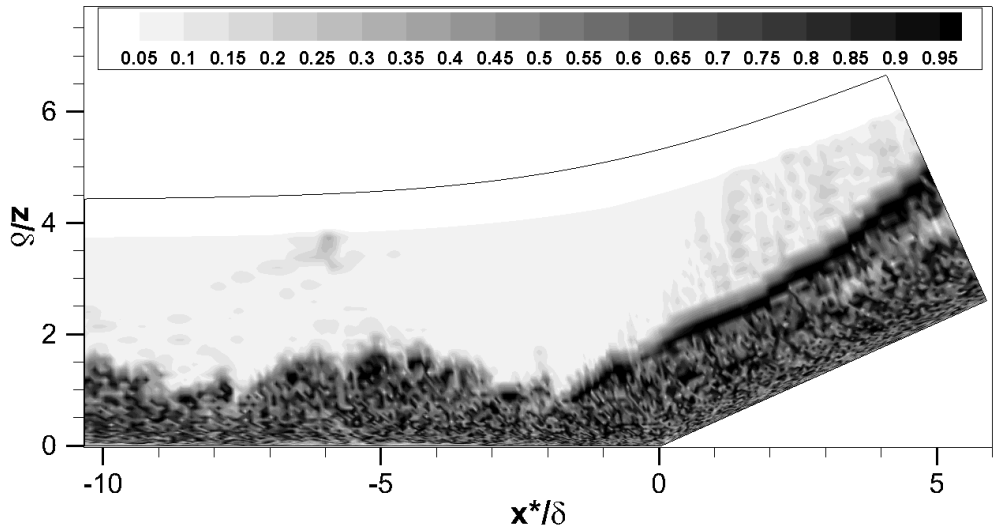

Figure 1. Nonlinearity index for compression ramp case without limiters

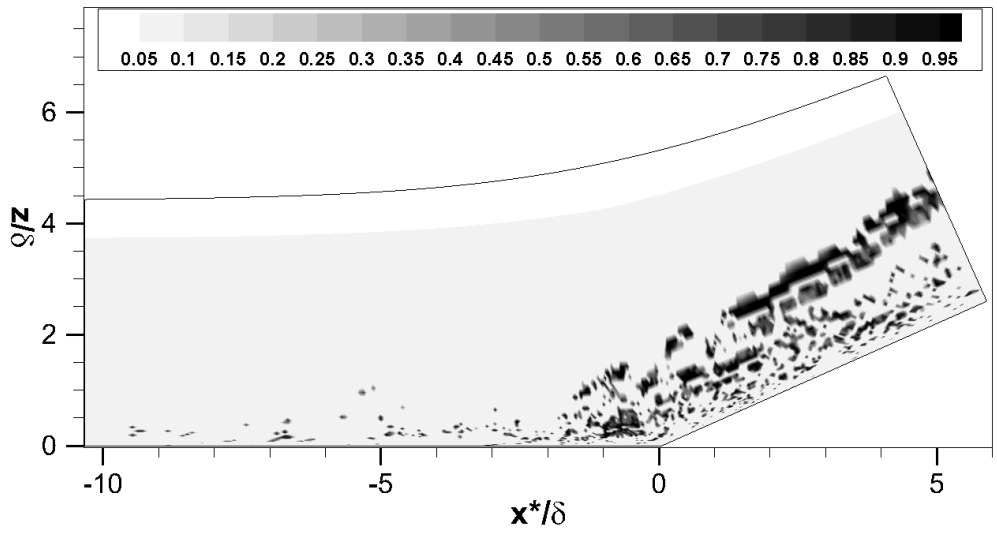

Figure 2. Nonlinearity index for compression ramp case with both absolute and relative limiters

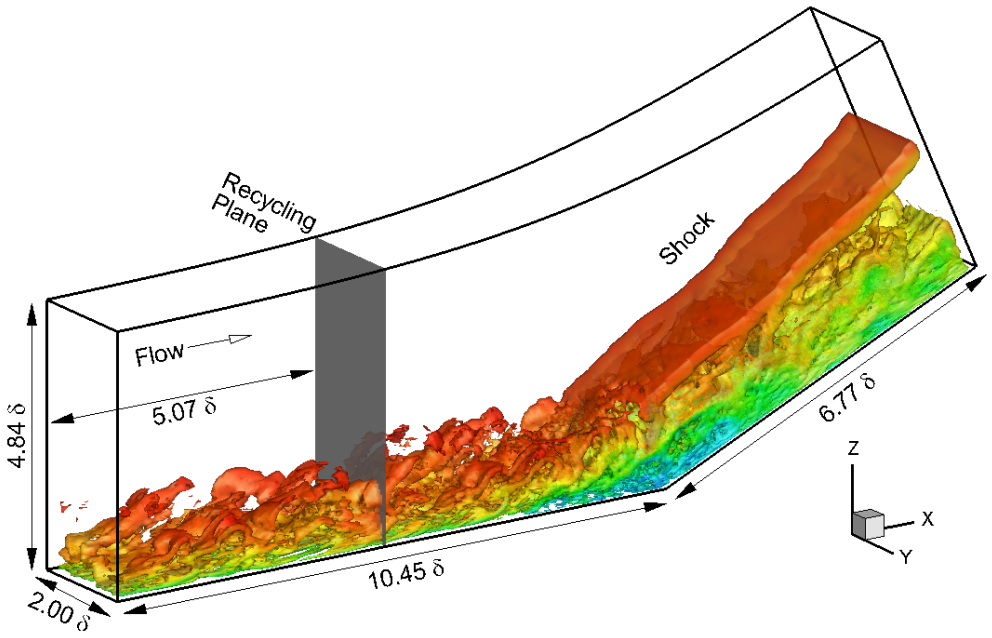

Figure 3. Computational domain with instantaneous flow field from LES visualized by isosurface $|\nabla\rho|\delta/\rho_\infty = 1.5$ with colored contour plot of normalized streamwise velocity, u/U_∞ ranging from -0.3 (blue) to 1 (red)

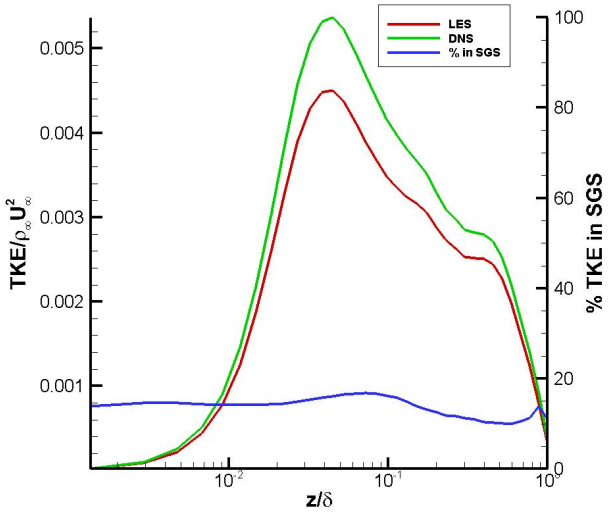

Figure 4. TKE profiles from turbulent boundary layer in DNS resolution, LES resolution, and percent energy modeled in subgrid scale terms

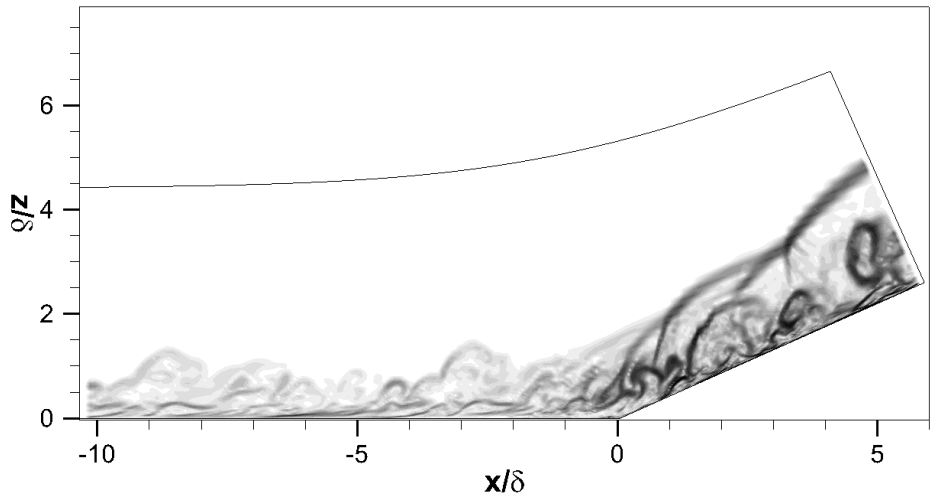

Figure 5. Instantaneous numerical schlieren for the LES. $NS = c_1 exp[-c_2(|\nabla\rho| - |\nabla\rho|_{min})/(|\nabla\rho|_{max} - |\nabla\rho|_{min})]$, **where** c_1 **and** c_2 **are constants**

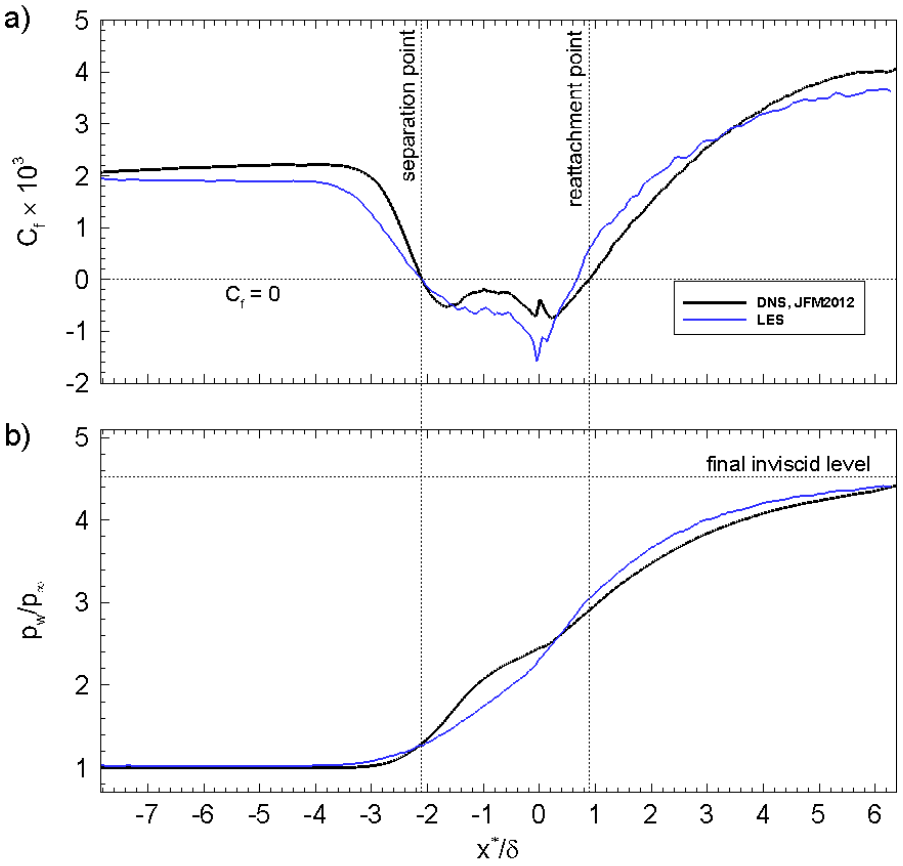

Figure 6. Time- and spanwise-averaged distribution of: (a) **skin friction coefficient** C_f**; and** (b) **wall-pressure**

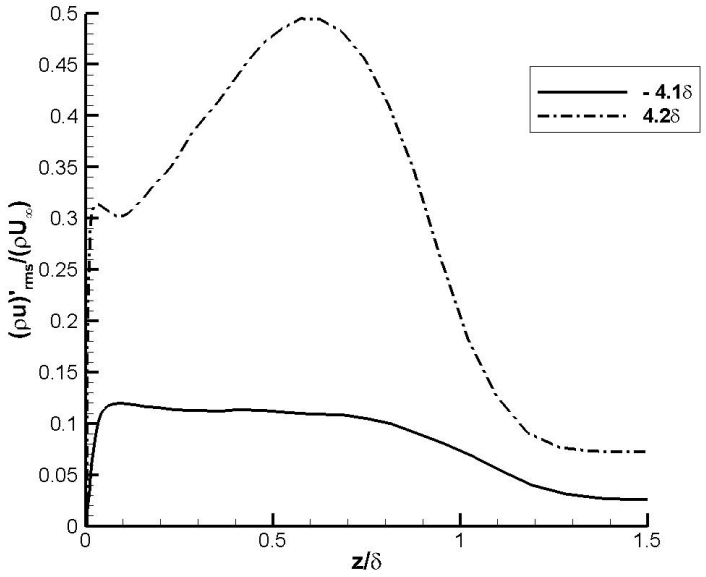

Figure 7. Time- and spanwise-averaged mass-flux turbulence intensities upstream ($x^*/\delta = -4.1$) and downstream ($x^*/\delta = 4.2$) of the interaction

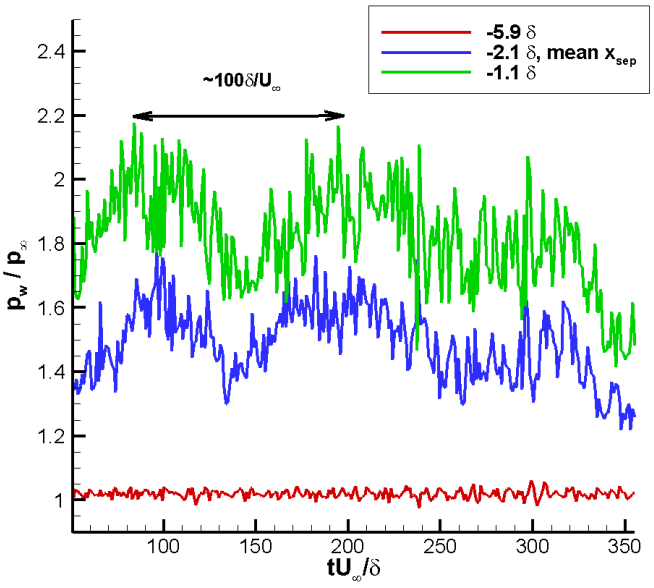

Figure 8. Wall-pressure fluctuations upstream ($x^*/\delta = -5.9$), at the mean separation point ($x^*/\delta = -2.1$), and inside the separation bubble ($x^*/\delta = -1.1$)